IAC-24-B4.7.15

SpEye: a CubeSat Technology Demonstration Mission for On-Orbit Inspection and Formation-Flying

Vincenzo Capuano[a]*, Fabio Saggiomo[b], Giuseppe Capuano[c], Enrico Vecchio[d], Giacomo Borelli[e], Gabriella Vittoria Maria Gaias[f], Camilla Colombo[g], Brunella Montanari[h], Riccardo Mantellato[i], Roberto Opromolla[j], Alessia Nocerino[k], Giuseppe Napolano[l], Michele Grassi[m], Giancarmine Fasano[n], Vito Fortunato[o], Luca Maria Stefano Pascali[p], Donato Chirulli[q], Caterina Noberasco[r], Giuseppe Leccese[s], Silvia Natalucci[t], Simone Illiano[u], Raffaele Votta[v], Marianna Rinaldi[w], Daniele Urban[x]

[a] *Techno System Developments S.R.L., Italy*, vcapuano@tsd-space.it
[b] *Techno System Developments S.R.L., Italy*, fsaggiomo@tsd-space.it
[c] *Techno System Developments S.R.L., Italy*, gcapuano@tsd-space.it
[d] *Techno System Developments S.R.L., Italy*, evecchio@tsd-space.it
[e] *Politecnico di Milano, Italy*, giacomo.borelli@polimi.it
[f] *Politecnico di Milano, Italy*, gabriella.gaias@polimi.it
[g] *Politecnico di Milano, Italy*, camilla.colombo@polimi.it
[h] *T4i, Italy*, b.montanari@t4innovation.com
[i] *T4i, Italy*, r.mantellato@t4innovation.com
[j] *Università degli Studi di Napoli "Federico II", Italy*, roberto.opromolla@unina.it
[k] *Università degli Studi di Napoli "Federico II", Italy*, alessia.nocerino@unina.it
[l] *Università degli Studi di Napoli "Federico II", Italy*, giuseppe.napolano@unina.it
[m] *Università degli Studi di Napoli "Federico II", Italy*, grassi@unina.it
[n] *Università degli Studi di Napoli "Federico II", Italy*, g.fasano@unina.it
[o] *Planetek Italia, Italy*, fortunato@planetek.it
[p] *Planetek Italia, Italy*, pascali@planetek.it
[q] *Planetek Italia, Italy*, chirulli@planetek.it
[r] *D-Orbit SpA, Italy*, caterina.noberasco@dorbit.space
[s] *ASI – Italian Space Agency, Italy*, giuseppe.leccese@asi.it
[t] *ASI – Italian Space Agency, Italy*, silvia.natalucci@asi.it
[u] *ASI – Italian Space Agency, Italy*, simone.illiano@asi.it
[v] *ASI – Italian Space Agency, Italy*, raffaele.votta@asi.it
[w] *ASI – Italian Space Agency, Italy*, marianna.rinaldi@asi.it
[x] *ASI – Italian Space Agency, Italy*, daniele.urban@asi.it
* Corresponding Author

Abstract

Space Eye (SpEye) is a two-satellite technology demonstration mission aimed at validating crucial technologies and methodologies essential for advanced on-orbit inspection and formation-flying. This initiative holds significant relevance for the development of future operational nano-satellite capabilities and missions.

The primary objective of the SpEye mission is to showcase the safe and cost-effective on-orbit inspection and mapping of a designated target satellite using an agile, autonomously maneuverable 6U CubeSat nanosatellite. Although the target satellite could be any resident space object, in the SpEye mission, it also serves as the deployer for the inspector satellite.

The key milestones of SpEye foresee the validation of several pivotal technologies, including: The free-flying 6U CubeSat inspector with autonomous maneuvering capabilities for orbiting in close proximity and imaging the target and deployer satellite; A versatile multispectral vision-based sensor system for autonomous navigation and inspection tasks; A Guidance, Navigation, and Control (GNC) processing unit implementing novel guidance and control schemes, fusing Global Navigation Satellite System (GNSS), Electro-Optical (EO), and Inertial Navigation System (INS) observations to ensure robust, precise, and reliable absolute and relative navigation; The propulsion system for the 6U CubeSat, enabling precise formation-keeping and proximity operations.

These technologies will also be leveraged to demonstrate the autonomous formation-flying of a 6U CubeSat alongside its deployer satellite, the autonomous rendezvous maneuvers between a 6U CubeSat and a resident space object and to validate several GNC algorithms.

The SpEye mission has been selected by the Italian Space Agency (ASI) in the framework of the call "Future CubeSat Missions", now part of the "Alcor" program. Led by TSD-Space (Techno System Developments S.r.l.), the mission comprises an all-Italian consortium, including D-Orbit, T4i (Technology for Propulsion and Innovation), Planetek Italia, Politecnico di Milano, and Università degli Studi di Napoli “Federico II”.

This paper describes the mission and presents a preliminary design overview of the critical subsystems of the free-flying inspector.

Keywords: Nanosatellite, CubeSat, On-Orbit Inspection, Formation Flying, Navigation, CDGNSS, Image Processing, Ground Segment as-a-service

Acronyms/Abbreviations

ADR	Active Debris Removal
ASI	Agenzia Spaziale Italiana
CDGNSS	Carrier-phase DGNSS
CT	Carrier Target
CRPO	Coarse Relative Parking Orbit
DGNSS	Differential GNSS
DOF	Degrees Of Freedom
EO	Electro-Optical
EOS	EO Subsystem
EPS	Electrical Power Subsystem
FF	Free Flyer
GNC	Guidance, Navigation & Control
GNSS	Global Navigation Satellite System
GS	Ground Segment
IDS	Integrated Data System
IMU	Inertial Measurement Unit
ION	InOrbitNow
IOS	In-Orbit Servicing
ISL	Inter-Satellite Link
ISS	International Space Station
LEO	Low Earth Orbit
LRF	Laser Range Finder
LWIR	Long Wave Infrared
OBC	On-Board Computer
PCB	Printed Circuit Board
PDT	Payload Data Transmission
SfM	Structure from Motion
SpEye	Space Eye
TM/TC	Telemetry & Telecommand
TRL	Technology Readiness Level
UHF	Ultra-High Frequency
VNIR	Visible and Near InfraRed

1. Introduction

In-orbit inspection has a broad range of critical applications, including routine spacecraft health assessments, emergency failure detection, and anomaly resolution. It also plays a vital role in debris characterization, small body exploration, and the monitoring of spacecraft operations. As the demand for precise space environment and asset monitoring increases, so does the need for advanced inspection technologies. Spacecraft formation flying and distributed space systems offer enhanced mission flexibility, cost efficiency, and performance compared to traditional monolithic spacecraft. In the context of IOS, autonomous orbital rendezvous is crucial for tasks like satellite assembly, ADR, and proximity operations involving diverse space systems.

Over the past decade, the global space community has made substantial advancements in IOS and ADR missions, addressing the increasing need for sustainable space operations. These mission architectures are essential for ensuring the long-term viability of space systems while offering significant economic benefits compared to traditional single-use platforms [1]. Key developments have focused on technologies such as autonomous rendezvous, docking, and sophisticated GNC systems, enabling both servicing and debris removal operations. Unlike earlier cooperative proximity operations, such as the Automated Transfer Vehicle (ATV) missions to the ISS [2], some IOS and ADR mission architectures present unique challenges due to the uncooperative nature of the target platforms. These platforms are often malfunctioning, non-functional, or tumbling in space, which complicates operations and requires advanced GNC technologies [3].

Since the late 1990s, proximity and robotic technology demonstrations, such as Orbital Express [1] and JAXA's ETSVII [4], have laid the groundwork for modern operations. Recently, Northrop Grumman’s MEV-1 and MEV-2 missions successfully docked with Intelsat satellites in geostationary orbit to extend their service life. In LEO, NASA’s OSAM-1 mission aims to service and refuel Landsat-7 [5], while ESA’s ClearSpace-1, slated for 2025, will deorbit a piece of debris called the VESPA payload adapter [6]. JAXA is also progressing with its CRD2 program [7] for debris removal technologies. Demonstration missions like RemoveDEBRIS [8] and Elsa-D [9] have also contributed to the advancement of debris removal technologies.

Within this evolving landscape, the use of free-flying nanosatellites for proximity operations is becoming increasingly relevant. Agile, low-cost platforms provide opportunities to validate key technologies for future IOS and ADR missions. Notable examples include Tyvak’s CPOD mission, which performed proximity operations using two 3U CubeSats in LEO [10], and NASA’s Seeker mission, which inspected the Cygnus spacecraft [11]. ESA’s e.inspector mission [12], initially designed to inspect the failed ENVISAT satellite, is now evolving to inspect the VESPA upper stage ahead of the ClearSpace-1 mission [13]. The Canadian CanX-4 and CanX-5 missions demonstrated formation flying and proximity operations using GNSS navigation in LEO [30]-[31].

In this context, Space Eye (SpEye) is a two-satellite technology demonstration mission designed to validate critical technologies for advanced on-orbit inspection and formation-flying. The mission consists of the Free Flyer and Carrier Target satellites, advancing capabilities essential for future nanosatellite operations.

SpEye will push the boundaries of nanosatellite GNC by utilizing advanced techniques, including GNSS code and carrier phase processing, electro-optical sensors [15]-[19], inertial measurements [20], and optimized fuel-efficient trajectories that prioritize collision avoidance and observational coverage.

SpEye Free Flyer is a 6U CubeSat developed by TSD-Space, while the Carrier Target is represented by an enhanced InOrbitNow (ION) platform developed by D-Orbit in the context of this mission.

The mission will validate and characterize compact, low-power components and technologies for proximity operations, all integral to the Free Flyer. Most of the Free Flyer's proximity operations will be conducted autonomously, using only the available navigation data, the onboard processor, flight software, and a highly integrated unit specifically designed for autonomous GNC.

More specifically, SpEye has the objective of validating the following technologies:

- The free-flying Nanosatellite Inspector, capable of autonomously flying around and imaging the main satellite from which it is deployed
- A Multispectral Vision-Based Sensor System, for autonomous navigation and inspection
- A GNC Processing Unit that integrates code-phase and carrier-phase GNSS, EO and Inertial Navigation System (INS) observations, for robust and accurate absolute and relative navigation
- A CubeSat Propulsion System that enables formation keeping and proximity operations.

At the same time, such technologies will be also used to demonstrate:

- Autonomous formation flying of a nanosatellite with its carrier
- Autonomous rendezvous of a nanosatellite with a resident space object.

An enhanced version of the D-Orbit ION platform will be utilized for the SpEye mission, specifically tailored to allow proximity operations with the Free Flyer. With respect to the previous eight ION satellites already launched, the enhancements will include an ISL and a propulsion system for proximity maneuvers.

Both the Free Flyer and Carrier Target satellite will employ an ISL to exchange navigation data (including GNSS) and image data collected by the electro-optical payload. These images, which will be preprocessed and compressed beforehand, will be shared between the satellites. Additionally, the Free Flyer will transmit this data to ground stations, where it will be further processed for diagnostic analysis.

The SpEye mission was selected by ASI as part of the "Future CubeSat Missions" call, now under the ALCOR [56] program. Led by TSD-Space, the mission is supported by an all-Italian consortium, including D-Orbit, T4i, Planetek Italia, Politecnico di Milano, and Università degli Studi di Napoli "Federico II". *Phase A* of the mission has been successfully completed, and the outcomes are presented in the following sections.

2. Mission Analysis and Design

The SpEye mission design focuses on defining phases to fulfill the mission objectives [21]. The SpEye Free Flyer will be deployed in orbit by the D-Orbit satellite carrier, ION, enabling a sequence of operations and demonstrations involving both the Free Flyer and the Carrier Target satellites. The operational orbit is determined by considering the requirement for debris mitigation, ensuring the CubeSat's uncontrolled reentry within 25 years. The chosen altitude of 535 km, in a circular orbit, resulted from a trade-off analysis that included reentry simulations, considering the Free Flyer's physical characteristics and varying levels of solar activity. This altitude ensures compliance with reentry requirements even under the worst-case scenario of low solar activity. Additionally, Local Times of the Ascending Node (LTAN) of 00:00 and 12:00 hours were preliminarily chosen through mission analysis to optimize lighting conditions during proximity operations. The mission is divided into pre-demonstration phases and demonstration phases, with the latter referred to as "Gates".

The pre-demonstration phases commence once the Free Flyer is released by the ION carrier. A sequence of maneuvers is then performed by the carrier to achieve a passively safe relative orbit in proximity to the Free Flyer during the so-called Release phase. Subsequently, a formation-keeping phase is conducted, during which the carrier executes the necessary maneuvers to maintain the passively safe relative orbit with the Free Flyer, forming an elliptical shape with a mean along-track separation of 15 km. The relative parking orbit achieved is characterized by E/I vector separation to ensure the safety of the formation [22]. In this phase, the Free Flyer completes its boots and commissioning of relevant subsystems before moving to the next phase.

The 15 km along-track distance was selected because of a tracking requirement to obtain separate tracking of the two satellites from ground, thereby facilitating the acquisition of coarse orbital determination products from Two-Line Elements (TLE). Following this, a far-range rendezvous phase is performed to reduce the separation between the two satellites, executing a spiral approach to a passively safe orbit with a mean along-track separation of 300 meters. The far-to-mid-range rendezvous is designed with initial and final positions in elliptical orbits, incorporating an E/I vector separation for passive abort safety, and using the spiraling strategy detailed in references [23]-[24] to maintain a high level of safety during the approach. Again, in this phase, the maneuvers are performed by the carrier satellite with the aim of saving the propellant resources of the Free Flyer platform for the subsequent scientific demonstration phases.

At the end of the far-to-mid-range rendezvous phase, the relative parking orbit with a mean along-track separation of 300 meters is achieved, and the primary operations of formation-keeping and relative orbit maneuvering are then taken over by the SpEye Free Flyer. From the relative parking orbit, in-orbit demonstrations of proximity operations and inspection begin.

In particular, three different gates of demonstrations are planned to fulfil mission objectives:

- **Gate I**: Demonstrate safe autonomous and *collaborative in-orbit inspection* of the host vehicle (chaser and target formation flying).
- **Gate II**: Demonstrate safe autonomous and *uncollaborative in-orbit inspection* of the host vehicle.
- **Gate III**: Demonstrate autonomous *rendezvous* of the free-flying inspector with its carrier.

The specific demonstrations planned for each gate are outlined in Tab. 1. It is important to note that, after each demonstration, the Free Flyer and Carrier Target satellites will return to the CRPO, before transitioning to the next planned demonstration. Additionally, the durations listed in Tab. 1 also account for the preliminary formation-keeping activities required for demo preparation. During this time, the platforms' subsystems are checked, data is analyzed, and the next operations are planned.

Phase	Distances	Duration
P.01 Transfer	N/A	N/A
P.02 Release	0-15 km	< 12 hours
P.03 Coarse formation keeping	15 km	7 days
P.04 Far-mid range rendezvouz	15 km to 300 m	~ 8 days
P.05 Relative parking orbit	300 m	7 days
P.06 Gate I Collaborative inspection	25-100 m	~ 5 days
• *Demo 1.1: Inspection with rotational collaboration of ION*		
P.07 Gate II Non-collaborative inspection	25-100 m	~ 25 days
• *Demo 2.1: Inspection with ION stable in RTN* • *Demo 2.2: Inspection with ION rotating (stable state) in RTN* • *Demo 2.3: Inspection with ION tumbling in RTN*		
P.08 Gate III Autonomous rendezvous	10-300 m	~ 10 days
• *Demo 3.1: Approach to v-bar hold point* • *Demo 3.2: Approach to inertial stable hold point* • *Demo 3.3: Approach to rotating hold point*		
P.09 Disposal operations	300 m – kms	< 10 days

Tab. 1. Concept of operations of the SpEye Mission.

3. **Free Flyer**

The Free Flyer will utilize a 6UXL CubeSat form factor, facilitating the integration of various subsystems. As illustrated in Fig. 1, the payload, along with the Communications Subsystem, is positioned at the front of the satellite, while the EPS, IDS, sensors, and actuators are housed in the rear. The satellite is equipped with two deployable 6U solar panels, leaving the two 3U faces available for antenna placement. The Propulsion Subsystem is centrally located, optimizing mass distribution within the spacecraft.

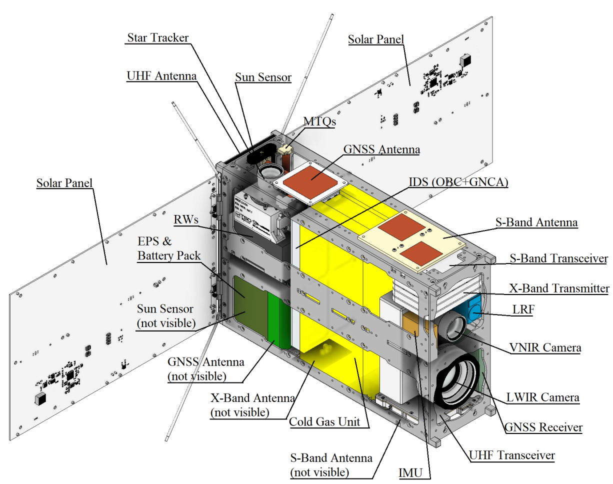

Fig. 1. SpEye Free Flyer Mechanical Configuration.

As shown in Fig. 2, the Free Flyer includes several key subsystems: EPS, OBC, GNC Accelerator, EOS, GNC Subsystem, Propulsion Subsystem, and Communications Subsystem. All primary sensors, actuators, and devices are connected to the OBC, which manages commands, processes data, and executes basic GNC functions. The OBC also interfaces with both the ground segment and the target satellite through the Communications Subsystem.

The EOS and LRF are directly connected to the GNC Accelerator, which handles computationally intensive tasks that require higher power and resources. The OBC and GNC Accelerator are integrated into a single enclosure, the IDS, and are connected via a high-data-rate interface. To preserve energy and minimize thermal output, the GNC Accelerator is powered down when these demanding computations are not needed.

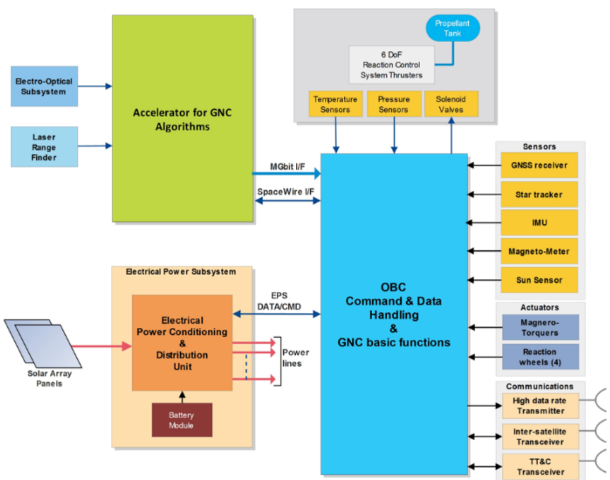

Fig. 2. SpEye Free Flyer Functional Architecture.

Tab. 2 summarizes the features of the SpEye Free Flyer.

Item	Description
Size	6UXL CubeSat form factor
Mass	12.3kg with margins
Battery Pack	100.8Wh and 180W nominal
Solar Array	36 Triple Junction cells (43.2W peak power)
Power Bus	12.0V to 16.8V with nominal 14.4V
GNC Sensors	Star Tracker 2 Sun Sensors IMU with Magnetometer GNSS Receiver Laser Range Finder Electro-Optical Subsystem
VNIR Camera	Non-scanning mode with 12 Mpx sensor 9 simultaneous acquired images (1 panchromatic + 8 spectral bands) 1365x1024 basic resolution (up to 4096x3072 using demosaicing algorithms) Spectral Range 400÷900nm Up to 12bit pixel depth Frame Rate up to 30 fps depending on the number of acquired bands
LWIR Camera	1024x768 resolution Spectral Range 8÷14µm Frame Rate up to 30 fps Thermal sensitivity < 50mK Dynamic Range > 100K
Image Processing Algorithms	Pre-processing (pixel equalization, Fixed-Pattern Noise (FPN) and Photo Response Non-Uniformity (PRNU) correction, etc) Lossless and Lossy Compression
Mass Memory	2x32Gbit chips, capable of storing about 2000 single-band VNIR images, 100 LWIR images and 900s of panchromatic video storage
LRF	Measurement frequency up to 25 Hz Wavelength ~1.55µm Range from 10m to 5km Accuracy (1σ) <=0.5m Resolution 0.1m
GNC Actuators	4 Reaction Wheels 3 Magnetorquers 6 DOF control via cold-gas thrusters
GNC Algorithms	Image Feature Detection and Tracking EO-based Pose Estimation GNSS-based orbit determination and relative navigation GNSS+EO–based relative navigation
Propulsion	6 DOF cold gas with R134a propellant Isp per nozzle ≥ 40s Thrust per nozzle ≥ 7mN Overall ΔV 20m/s
Communications	UHF for TM/TC, uplink @9.6 kbit/s and downlink @19.2 kbit/s S-Band for ISL, up to 512 kbit/s X-Band for PDT, up to 200 Mbit/s

Tab. 2. Summary of the SpEye Free Flyer features.

3.1 Electrical Power Subsystem

The Free Flyer's EPS has been designed to meet specific performance requirements for both power generation and energy storage, based on the power budget analyses conducted during *Phase A*, and the satellite's operational scenarios. The system consists of the following components:

- Two deployable 6U solar panels, along with a 2U solar panel placed on the back of the CubeSat. This solution is capable of providing the satellite with up to 39W at End-of-Life (EoL).
- A battery pack, which includes 3 strings of 4x 18650 cells each. One string is nominally in standby mode, as it is used as redundancy in case of failure of one of the other strings. This solution features a nominal energy storage capacity of 100Wh, with a maximum deliverable power of 180W, which is more than sufficient to supply all the Free Flyer Subsystems.
- A Power Conditioning & Distribution Unit (PCDU), provided with Maximum Power Point Tracking (MPPT), which interfaces with the solar panels, the battery pack, and all the subsystems.

3.2 Integrated Data System

The Free Flyer Integrated Data System, depicted in Fig. 3 and Fig. 4, is the brain of the SpEye platform. It consists of:

- OBC, which performs Command & Data Handling (CDH), along with basic GNC functions.
- GNC Accelerator, which is a module dedicated to the acceleration of the GNC algorithms based on the LRF and the EOS.

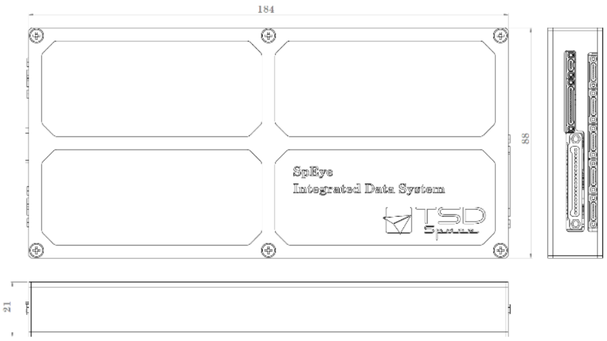

Fig. 3. Envelope of the SpEye Free Flyer IDS: it integrates the OBC and the GNC Accelerator boards in a single envelope, limiting the overall volume of the system.

Fig. 4. Computer Aided Design (CAD) representation of the SpEye Free Flyer IDS.

Only the EOS and the LRF are directly interfaced with the GNC Accelerator, while the remaining GNC sensors, actuators, and propulsion subsystem components are connected to the OBC, as shown in Fig. 5. This configuration allows the GNC Accelerator to be powered only during operation modes that require computationally intensive algorithms, such as image processing and data fusion. As a result, the overall power consumption of the data system is significantly reduced during less demanding operational modes.

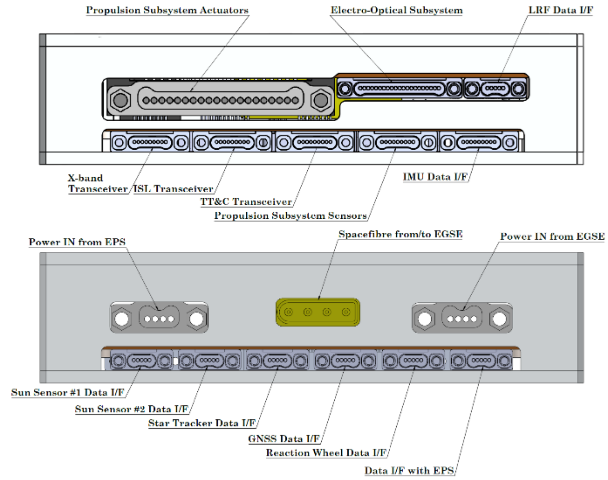

Fig. 5. Interface Connectors on both OBC and GNC Accelerator in the SpEye Free Flyer IDS: only the EOS and the LRF are connected to the GNC Accelerator

Two data interfaces are planned between the OBC and the GNC Accelerator: a high-speed MultiGbit interface operating at over 1 Gbit/s for the real-time transfer of images from the GNC Accelerator to the OBC, and a SpaceWire interface with up to 100 Mbit/s throughput, designed for low-latency exchange of sensor and actuator data between the two systems.

3.3 Electro-Optical Subsystem and Laser Range Finder

The Free Flyer's Electro-Optical Subsystem includes two cameras, and is coupled with a LRF. The LRF is a compact unit capable of measuring distances along its axis up to 2 km with sub-meter accuracy (1σ). The EOS, shown in Fig. 6, is derived from a product developed and qualified by TSD-Space with a TRL of 9, as part of the ArgoMoon program. For the SpEye mission, TSD-Space will customize this camera, primarily through modifications to the optical heads.

The camera used in ArgoMoon features two optical heads, each with a CMV12000 sensor and shared electronics. One optical head is equipped with a 393mm focal length lens for a narrow field of view, while the second head has a focal length of about 22mm for a wide field of view.

In SpEye, the first optical head will be repurposed for multispectral imaging in the VNIR bands, while the second head will be adapted for thermal infrared imaging in the LWIR band. Both heads will be equipped with wide-field optics to ensure proper target satellite visibility, even at close range. The VNIR sensor will remain the CMV12000, now outfitted with a state-of-the-art multispectral filter, while the LWIR sensor will be upgraded to the PICO 1024 Gen2. Additionally, the entire camera system will be made more compact than its ArgoMoon counterpart to facilitate integration within the CubeSat.

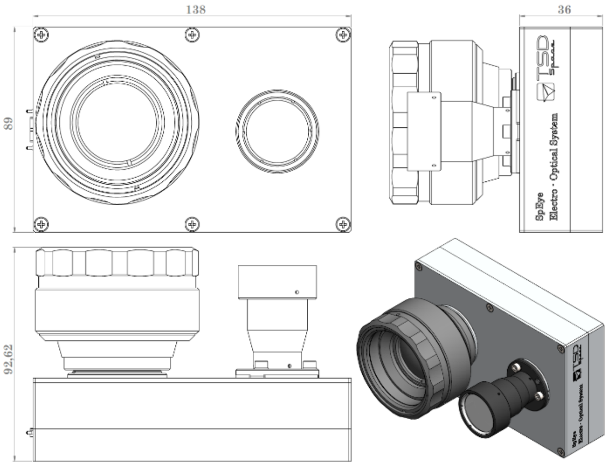

Fig. 6. SpEye Free Flyer EOS: the VNIR and LWIR cameras are located on a single rigid PCB, making the system more compact than the ArgoMoon system already developed by TSD.

Fig. 7 illustrates the PCB layout of the EOS.

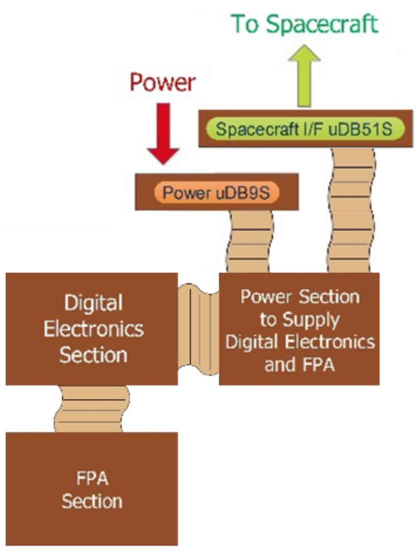

Fig. 7. SpEye Free Flyer EOS PCB layout.

3.4 Propulsion Subsystem

The Free Flyer propulsion subsystem enables 6 DOF for proximity operations maneuvers and reaction wheel desaturation. The system architecture has been developed to meet envelope constraints, mass limitations, and mission-specific requirements. Based on these requirements, a system analysis was carried out to obtain the initial performance parameters of the propulsion subsystem, according to the following relation (1):

$$m_{PROP} = m_i\left(1 - e^{-\frac{\Delta v}{I_{sp}g}}\right) \qquad (1)$$

Where m_{PROP} is the propellant mass, m_i is the initial mass of the satellite, and Δv is the overall change in velocity required to perform all the maneuvers, along all axes. The distribution of delta-v across the individual axes provided important information for the optimized inclination of the nozzles. I_{sp} is the specific impulse of the propellant and g is the gravity acceleration. The desired thrust levels led to a preliminary definition of the mass flow rate, a preliminary design of the nozzle, and a definition of the involved pressure levels, according to Equations (2) and (3):

$$T = \dot{m} I_{sp} g \qquad (2)$$

$$\dot{m} = \frac{p_c A_t}{c^*} \qquad (3)$$

Where T is the thrust, $\dot{m}$ is the propellant mass flow rate, p_c is the pressure upstream the nozzle, A_t is the throat area, and c^* is the characteristic velocity.

The propellant selected for this propulsion subsystem is R134a, a biphasic fluid that offers several advantages, including: i) moderate storage pressure, and ii) high density, which leads to a more compact system and higher impulse density. Additionally, R134a is a non-toxic, non-flammable fluid, enabling safe test procedures for personnel. It is also environmentally friendly, with a zero Ozone Depletion Potential (ODP) and a moderate Global Warming Potential (GWP).

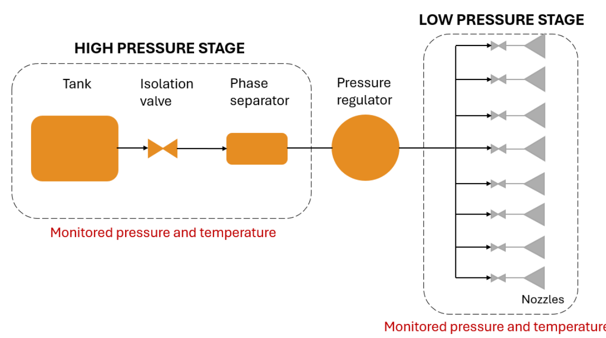

Fig. 8. SpEye propulsion subsystem fluidic line schematics.

As illustrated in Fig. 8, the propulsion subsystem fluidic line consists of a high-pressure stage and a low-pressure stage, separated by a pressure regulator that reduces the pressure to the target level before the propellant reaches the nozzles. The high-pressure stage includes: i) the tank, where the propellant is stored; ii) an isolation valve that acts as a safety barrier for the rest of the propulsion subsystem; and iii) a phase separator, which guarantees a fully gaseous mass flow rate (quality = 1) regardless of the inlet conditions. The low-pressure stage comprises eight nozzles and their corresponding, independent, valves. A preliminary component selection has been carried out, considering factors such as accuracy, power, chemical compatibility, mass, dimensions, and lead times, to ensure that the project deadlines are met.

The upcoming objectives of the propulsion subsystem for the next phases of the project include conducting a preliminary design and a testing campaign on a breadboarding model to verify the system's performance from structural, fluidic, and propulsion perspectives.

3.5 Communications Subsystem

The Free Flyer Communications Subsystem allows the satellite to:

- Receive commands from the ground and transmit telemetry data back, facilitating two-way communication (TM/TC) between the satellite and the ground station
- Establish an ISL with the Carrier Target satellite
- Send image and video data, coming from the EOS to ground (PDT).

The ISL enables the exchange of GNSS and image data with the target satellite. GNSS data from both platforms can then be used by the Free Flyer for DGNSS purposes, enhancing the accuracy of relative position estimation.

TM/TC are managed via a UHF transceiver, supported by four dipole antennas, which are visible on the back of the satellite in Fig. 1. Both the Free Flyer and the Carrier Target are equipped with an S-band transceiver that manages the ISL, along with four corresponding antennas: two for transmission (TX) and two for reception (RX), mounted on opposite sides of each satellite. This configuration ensures uninterrupted communication between the transceivers, regardless of the relative attitude of the two satellites.

Finally, PDT is handled by an X-band transceiver, paired with a single X-band antenna.

4. Guidance, Navigation & Control

The Free Flyer GNC Subsystem comprises the following sensors and actuators:

- A Star Tracker
- Two Sun Sensors on opposite sides
- An IMU, which is also provided with a Magnetometer
- A GNSS receiver, coupled with two antennas on opposite sides to maximize coverage
- Four Reaction Wheels in tetrahedral configuration, thus providing redundancy
- Three Magnetorquers on three orthogonal axes, which will be used especially to hinder the reaction wheels saturation

4.1 Navigation

illustrates the preliminary functional architecture of the navigation subsystem of the Free Flyer, which includes different sensors and processing modules dedicated to absolute and relative navigation.

Absolute navigation will be mainly based on the processing of GNSS and Star Tracker observations collected by the Free Flyer. Other sensors such as an IMU, a magnetometer and sun sensors will also be integrated and their measurements utilized to improve continuity, integrity and accuracy of the absolute navigation solution. The on-board navigation filter will be based on the design described in [20] and on the previous development by TSD-Space of the system VINAG, summarized in [25].

In relative navigation, different sensors and different types of filtering couplings are adopted in different navigation modes, as defined in Tab. 3.

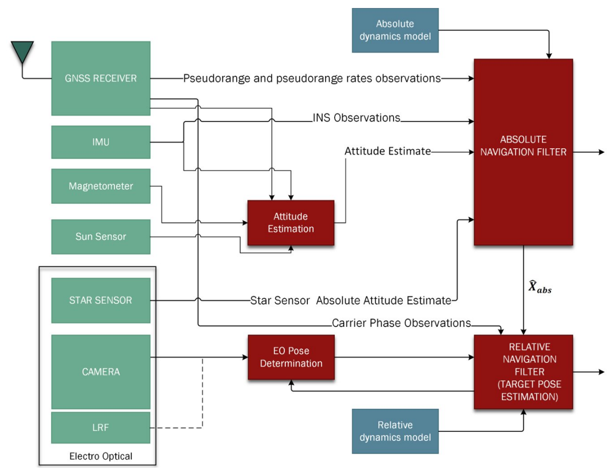

Fig. 9. SpEye Free Flyer Navigation Algorithm Functional Architecture.

The baseline solution is *Nav Mode 1*, based on CDGNSS performed using GNSS observations collected on board both Free Flyer and Carrier Target, and shared through the ISL. A hybrid approach will be implemented, where the spacecraft performs navigation on board autonomously and periodically sends collected raw GNSS data to ground stations for more precise processing and error correction. This approach balances autonomy with the benefits of ground-based processing.

In *Nav Mode 2*, combined use of EO sensors and DGNSS measurements (or CDGNSS if available) is foreseen. Such operative mode is conceived with the idea that, during collaborative inspection, when data exchange is possible through the ISL, differential GNSS measurements can help improving the accuracy of a 6-DOF relative state estimation filter, thus helping the 3D reconstruction task. In fact, ranging measurements can be used both to aid the purely EO-based pose estimation task and as independent measurements within the correction step of the navigation filter. This latter point is relevant, since it allows injecting in the filter a measurement term to directly correct the relative velocity terms within the state vector. Indeed, in conventional EO-based relative navigation schemes, this correction occurs only indirectly through the relative position measurements obtained by a loosely coupled pose estimation pipeline. Another advantage of such an approach is that DGNSS and LRF measurements can be used also during eclipse (the former without strict constraints on the Free Flyer attitude pointing).

Regarding the processing of measurements from the camera, two sub-modes are foreseen depending on the apparent size of the target on the image plane. Indeed, if the target projection occupies a region smaller than a threshold only line-of-sight (LOS) measurements are available, and the relative state estimation filter can only provide information on the translational dynamics. If the target projection overcomes a threshold, a dedicated image processing pipeline allows extracting a set of natural/geometric features of the target and matching them with their known 3D position vector in target body coordinates.

The resulting perspective-n-points problem is solved through a combination of analytical and numerical solvers to perform coarse pose estimation and refinement. The measured pose parameters are then input into the filter thus allowing full 6 DOF relative state estimation. In both the 3 DOF and 6 DOF cases, a Multiplicative Extended Kalman Filter (MEKF) is selected as filtering scheme. More details on the selected strategy and its preliminary results (obtained through numerical simulations within a dedicated virtual environment including a synthetic image simulator) can be found in [18].

In *Nav Mode 3*, a more robust and accurate CDGNSS solution is foreseen, based on the design proposed in [14] and [15], utilizing the assistance of EO observations. Features extracted from the image frame and matched with a stored model (see [16],[17]) are tightly integrated with GNSS observations to enhance the probability of successful integer ambiguity resolution, shorten the time required for resolution, and ultimately improve the achievable relative positioning accuracy.

Finally, in *Nav Mode 4*, a purely EO-based relative navigation architecture is implemented to demonstrate rendezvous capabilities towards a non-cooperative and non-collaborative target. Such architecture is analogous to the one conceived for Nav Mode 2. Indeed, it still relies on the integration of different measurements (namely ranging data from the LRF and LOS or pose measurements from the camera depending on the target distance), within a MEKF.

Since CDGNSS measurements are not available, the EO-only mode cannot operate during eclipse, thus posing stricter time constraints on the execution of rendezvous maneuvers. Indeed, LRF measurements alone are not enough for the correction of the entire translational relative navigation state. Again, details and preliminary results can be found in [18].

	CDGNSS	Visual Camera	LRF	Loose Coupling	Tight Coupling
Nav Mode 1 CDGNSS only	✓				✓
Nav Mode 2 CDGNSS-EO Multisensor	✓	✓	✓	✓	
Nav Mode 3 EO Assisted CDGNSS	✓	✓	✓		✓
Nav Mode 4 EO only		✓	✓	✓	

Tab. 3. Navigation Modes envisaged in the context of the SpEye Mission.

4.2 Guidance and Control

This subsection describes the guidance and control strategies adopted to enable the inspection and rendezvous demonstrations. Specifically, we focus on the approaches developed for the non-collaborative inspection trajectory design and the autonomous close-range rendezvous. Both approaches are characterized by a high emphasis on operational safety. Great care was taken to incorporate passive abort safety features into the proximity trajectories. This means that the satellites, while following these relative trajectories, remain collision-free for a specified duration (in our case, 12 hours), even if no collision avoidance maneuvers are executed. Consequently, in the event of major failures or contingencies leading to a total loss of control, collisions are still avoided.

The non-collaborative trajectory design is based on an algorithm proposed in [42]. The inspection design of the SpEye mission introduces a distinctive methodology, using information cost as a key metric to guide motion planning. The optimization of the inspection trajectory is governed by the metric expressed in Equation (4):

$$J = IC + a\Delta\delta\boldsymbol{\alpha}^T W_{\delta v}\, a\Delta\delta\boldsymbol{\alpha} \qquad (4)$$

The term IC represents the "Information Cost", which quantifies the quality of observations acquired along a specific trajectory in terms of mapping coverage of the target features. The second term is a cost metric that represents the control effort required to transition from the current relative inspection trajectory to the next one. The term $W_{\delta v}$ is used to weigh the transfer cost with the information cost in the optimization process. A sampling-based motion planning approach is developed, which utilizes a sample of passive abort-safe trajectories (see reference [21]) and employs a sequential greedy algorithm to construct a sequence of relative orbits that minimize the cost function. An example of such a sequence, which utilizes relatively stable orbits to observe the features of a stable target (Demo 2.1), is shown in Fig. 10. The transfer strategy used to move from one inspection trajectory to the next is similar to the strategy employed for close-range rendezvous (Gate III), and it is described in the following section.

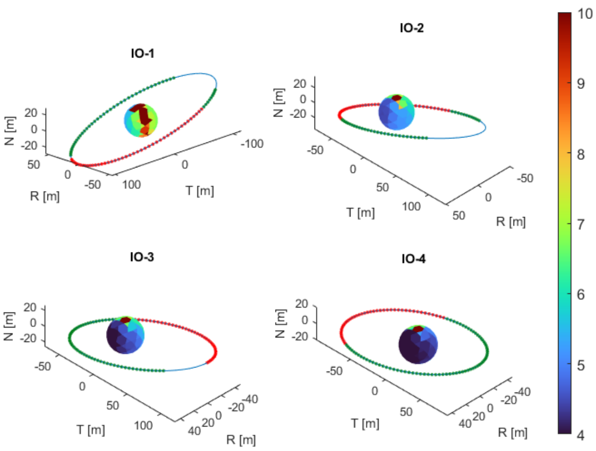

Fig. 10. Sequence of relative trajectories obtained considering non-drifting passively safe orbits to observe the feature of a target stable in RTN.

The guidance and control strategy for close-range rendezvous is based on the algorithm developed in references [43] and [44]. In each demonstration, the Free Flyer begins from the CRPO and transfers to a closer, passively safe hold point orbit (shown in magenta in Fig. 11). Following this, the close-range rendezvous begins, bringing the Free Flyer to the predefined hold point specified by the demonstration (see Tab. 1). Subsequently, the Free Flyer is transferred back from the hold point to the CRPO.

The transfers are designed using an optimization-based guidance and control method that employs a sequential convex programming algorithm. Safety constraints, including passive abort safety and active collision safety, are enforced throughout the transfer, while fuel minimization is also taken into account. For more details on the formulation of the constrained optimal control, please refer to references [43] and [44]. An example of an open-loop guidance trajectory for both the forward and return trajectories is shown in Fig. 11 for Demo 3.2, resulting in a delta-v expenditure of 0.39 m/s.

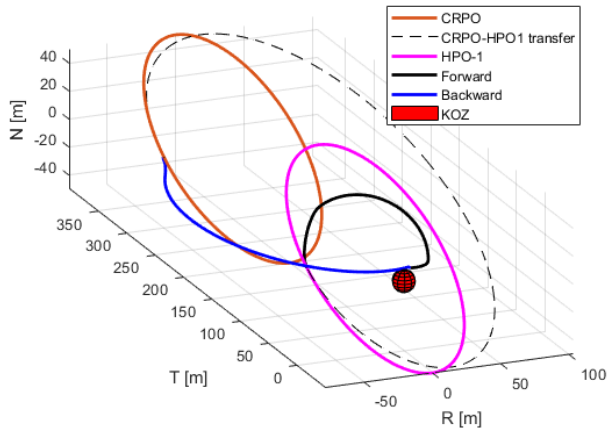

Fig. 11. Demo 3.2 open-loop trajectories.

5. Inspection Data Processing

A key innovation of the SpEye mission is its advanced approach to analyzing inspection data through 3D reconstruction and thermal diagnostics. These technologies allow for a detailed assessment of a satellite's structural integrity and thermal health, ensuring comprehensive inspection capabilities. The system leverages two primary sensors onboard the Free Flyer: a multispectral optical sensor for precise 3D reconstruction of the target satellite and a long-wave infrared (LWIR) sensor for thermal diagnostics.

5.1 3D Reconstruction

3D reconstruction using SfM is adopted for assessing the overall structural integrity of the satellite. SfM typically relies on a series of 2D images to infer 3D structures by tracking feature points across multiple views. The primary sensor for 3D reconstruction is the *VNIR CMV12000* image sensor described in Section 3.3. However, integrating laser range finder (LiDAR) data can enhance the process by directly providing depth information, which can significantly improve accuracy in certain conditions, such as low-visibility environments.

LRF measurements offer direct 3D spatial data, and this can complement the image-based SfM by providing distance points. The combination of both datasets (LRF- and image-based) can improve the robustness of the reconstruction, especially in scenarios where visual features are sparse or occluded.

During the inspection phases, the sensor captures images at varying distances, typically in the range of 30 to 50 meters from the target satellite, optimized for achieving maximum coverage and accuracy. The images are processed incrementally, starting with the acquisition phase, followed by correspondence search, 3D point cloud reconstruction [47]-[49], and finally surface reconstruction [50], [54]. The resulting 3D model is then compared to the ground truth model to identify any surface irregularities, potential damage or other anomalies.

5.2 Thermal Inspection

The The SpEye Free Flyer will capture long-wave infrared (LWIR, 8-14 µm) thermal data of the Target satellite to assess its thermal state and identify potential anomalies. This data will provide insights into the satellite's thermal behavior, contributing to comprehensive health monitoring.

The diagnostic workflow involves analyzing the temperatures of specific Regions of Interest (ROI) in the LWIR images, corresponding to key Points of Interest (POI) on the satellite. Measured temperatures are compared to nominal ranges, with alerts triggered for deviations (Fig. 12). The analysis combines Infrared Thermography (IRT) techniques and LWIR sensor data, including both real-time and post-processing steps. The main stages include [46]:

1. *Noise Reduction*: Improve IR image quality by reducing noise.
2. *Faulty Pixel Compensation*: Detect and correct for dead or overheated pixels.
3. *Image Enhancement*: Refine image details for better thermal analysis.
4. *ROI Identification*: Use image processing to locate key thermal regions.
5. *Emissivity Assignment*: Assign emissivity values based on material properties.
6. *Reflected Temperature Evaluation*: Account for external thermal radiation.
7. *Temperature Calculation*: Combine emissivity and reflected temperature to compute accurate surface temperatures.

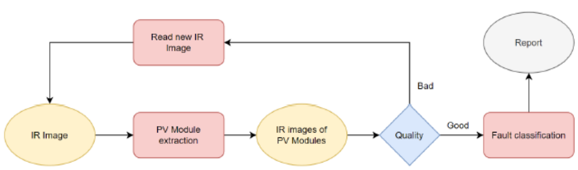

Fig. 12. Thermal Analysis Workflow.

One key application is the inspection of satellite solar panels. This method involves detecting Photovoltaic (PV) modules in thermal images and classifying faults, such as open circuits or overheated cells, based on temperature data. Techniques like AI, originally developed for UAV-based solar panel inspections, can be adapted for space. The IEC TS 62446-3 Standard guides the development of fault detection algorithms [55].

6. **Ground Segment**

The SpEye Ground Segment (GS) architecture is designed for flexibility, supporting both cloud-based and physical hardware deployments as needed. It prioritizes mission requirements, system reliability, performance optimization, and cost-efficiency, while minimizing development risks. The GS development emphasizes the reuse of proven components, with targeted upgrades where necessary.

Referred to as the integrated Ground Segment (iGS), it consists of four main functional components, as shown in Fig. 13:

1. *Carrier Target Flight Operations Segment (CT-FOS)*
   - Control and Monitoring: Manages the Target satellite using D-Orbit's proprietary system, customized for SpEye operations and data analysis.
2. *Mission Control Software*: Utilizes Aurora to manage and command the ION fleet.
3. *Free Flyer Ground Segment (FF GS)*
   - Control and Monitoring: Manages the cubesat using Planetek's proprietary system, tailored for SpEye operations and data management.
   - Software: Employs Ermes, a customizable Mission Control System (MCS) supporting various ground station providers, mission information bases, and scheduling protocols.
4. *SpEye Mission Operations Center (MOC)*
   - Operations Coordination: Defines and dispatches operations and schedules to CT-FOS and FF-GS
   - Telemetry Management: Collects telemetry from Aurora and Ermes, issues commands based on consortium input, delivers data to the Mission Exploitation Segment, and interfaces with third-party services.
5. *SpEye Mission Exploitation Segment (MES)*
   - Dashboard Provision: Processes and analyzes mission data for further exploitation, supporting post-mission evaluation and external service integration.
   - Data Highlighting: Supports estimation and post-processing of mission data

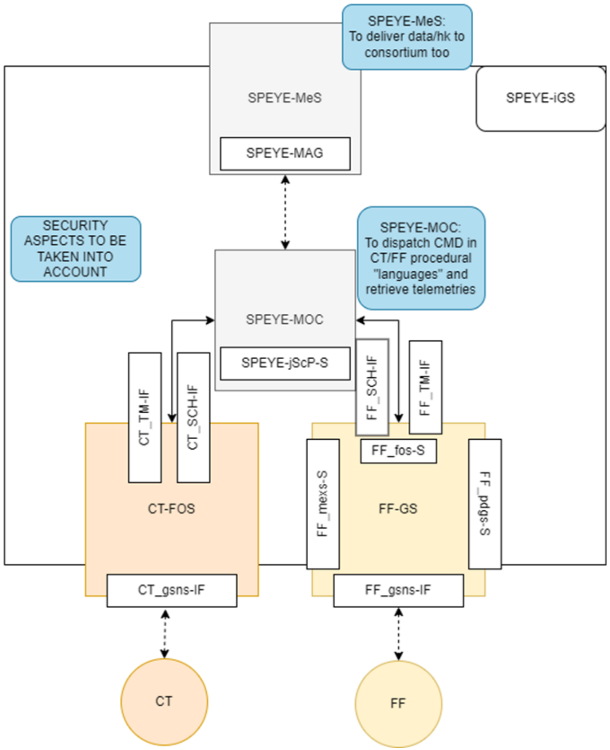

Fig. 13. SpEye Integrated Ground Segment Preliminary Design.

6.1 Formation Control

The Free Flyer Ground Segment is responsible for the monitoring and control of the Free Flyer spacecraft, encompassing imaging data acquisition, processing, archiving, and diagnostic analysis. It manages mission planning to prevent operational conflicts based on predefined scenarios and ensures the quality of both operations and data products. To maintain payload performance and ensure mission success, continuous monitoring, calibration, and validation activities are conducted.

From a functional perspective, the main components of the Free Flyer Ground Segment, referred to as the Free Flyer Control System (FFCS), are outlined below and depicted in Fig. 14:

1. *Mission Operations Center (MOC)*, comprising:
   a. *Flight Operations Segment (FOS)*: Oversees all flight operations of the Free Flyer spacecraft, including both spacecraft and payload planning activities.
   b. *Payload Data Ground Segment (PDGS)*:Manages payload data, including calibration, validation, quality control, and end-to-end system performance assessment.
   c. *Mission Exploitation Segment (MES)***:** Provides a consultation platform, offering a unified access point for internal users (e.g., mission analysts) and external stakeholders (e.g., agencies) to retrieve Free Flyer inspection campaign products and related analytics.
2. *Ground Stations Network (GSN)*: Supports communication and data transfer between the Free Flyer and ground systems.

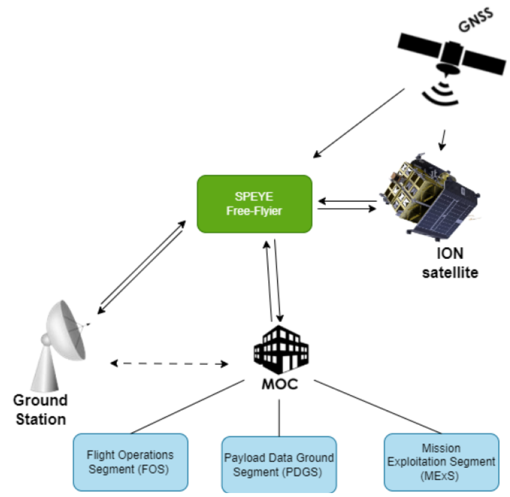

Fig. 14. SpEye Free Flyer GS Architecture.

7. Conclusions

The SpEye mission is a promising initiative that aims to demonstrate key technologies for advanced on-orbit inspection and formation flying using nanosatellites. By validating GNC systems, alongside innovative multispectral and thermal imaging techniques, SpEye is poised to contribute to the growing field of nanosatellite-based proximity operations. The integration of GNSS-based navigation with optical and inertial data will enable precise and autonomous maneuvering, essential for future IOS and ADR missions.

At this time, the mission is entering *Phase B*, focusing on refining the system architecture and finalizing the design of critical subsystems. In later phases, SpEye will have the potential to demonstrate advanced inspection techniques that could set the stage for future operational missions, enhancing the sustainability and resilience of space systems.

Acknowledgements

The project "Space Eye (SpEye)" is supported by ASI, Contract ASI n. 2023-1-I.0, Codice Identificativo Gara (CIG) 9352506C18, Codice Unico di Progetto (CUP) F83D23000000005.

References

[1] Flores-Abad, Angel, et al. "A review of space robotics technologies for on-orbit servicing." *Progress in aerospace sciences 68* (2014): 1-26.

[2] European Space Agency (ESA). "ATV – Automated Transfer Vehicle." Retrieved on 16 Sept 2024, from *https://www.esa.int/Science_Exploration/Human_and_Robotic_Exploration/ATV/Automated_Transfer_Vehicle* (2020)

[3] Shan, Minghe, Jian Guo, and Eberhard Gill. “Review and comparison of active space debris capturing and removal methods.” *Progress in aerospace sciences 80* (2016): 18-32.

[4] Kawano, Isao, et al. “Result of autonomous rendezvous docking experiment of engineering test satellite-VII.” *Journal of Spacecraft and Rockets 38.1* (2001): 105-111.

[5] Vavrina, Matthew A., et al. “Safe rendezvous trajectory design for the restore-l mission.” *Advances in the Astronautical Sciences 168* (2019): 3649-3668.

[6] Biesbroek, Robin, et al. “The clearspace-1 mission: ESA and clearspace team up to remove debris.” *Proc. 8th Eur. Conf. Sp. Debris*. 2021.

[7] Yamamoto, Toru, et al. “Pave the way for active debris removal realization: Jaxa commercial removal of debris demonstration (crd2).” *8th European Conference on Space Debris*. 2021.

[8] Forshaw, Jason L., et al. “The active space debris removal mission RemoveDebris. Part 1: From concept to launch.” *Acta Astronautica 168* (2020): 293-309.

[9] Forshaw, Jason, et al. “The ELSA-d End-of-life debris removal mission: mission design, in-flight safety, and preparations for launch.” *Proceedings of the Advanced Maui Optical and Space Surveillance Technologies Conference*, 17-20 September, 2019, Maui, Hawaii. 2019.

[10] Roscoe, Christopher WT, Jason J. Westphal, and Ehson Mosleh. “Overview and GNC design of the CubeSat Proximity Operations Demonstration (CPOD) mission.” *Acta Astronautica 153* (2018): 410-421.

[11] Pedrotty, Samuel, et al. “Seeker free-flying inspector gnc system overview.” *American Astronautical Society Annual Guidance and Control Conference* (AAS GNC 2019). No. JSC-E-DAA-TN64849. 2019.

[12] Team, E. C. “e. Inspector CDF Study Report-Assessment of an ENVISAT Imaging Mission as a Precursor to a Potential ENVISAT Deorbit”. *Tech. rep., European Space Agency (ESA)*, 2017.

[13] Silvestrini, Stefano, et al. “Design of robust passively safe relative trajectories for uncooperative debris imaging in preparation to removal.” *2020 AAS/AIAA Astrodynamics Specialist Conference*. 2020.

[14] Capuano, Vincenzo, et al. “DGNSS-vision integration for robust and accurate relative spacecraft navigation.” *Proceedings of the 32nd International Technical Meeting of the Satellite Division of The Institute of Navigation (ION GNSS+ 2019)*. 2019.

[15] Capuano, Vincenzo, Alexei Harvard, and Soon-Jo Chung. “On-board cooperative spacecraft relative navigation fusing GNSS with vision.” *Progress in Aerospace Sciences 128* (2022): 100761.

[16] Capuano, V., Alimo, S. R., Ho, A. Q., & Chung, S. J. (2019). Robust features extraction for on-board monocular-based spacecraft pose acquisition. In *AIAA Scitech 2019 Forum* (p. 2005).

[17] Harvard, A., Capuano, V., Shao, E. Y., & Chung, S. J. (2020). Spacecraft pose estimation from monocular images using neural network based keypoints and visibility maps. In *AIAA Scitech 2020 Forum* (p. 1874).

[18] Opromolla, Roberto, et al. “Electro-Optical based relative navigation for close-range inspection and rendezvous in the SpEye CubeSat-based mission.” *AIAA SCITECH 2024 Forum*. 2024.

[19] Napolano, Giuseppe, et al. “A multi-sensor optical relative navigation system for small satellite servicing.” *Acta Astronautica 207* (2023): 167-192.

[20] Capuano, Vincenzo, et al. “GNSS/INS/Star tracker integration for Real-time on-Board autonomous orbit and Attitude determination in LEO, MEO, GEO and beyond.” *68th International Astronautical Congress (IAC)*. 2017.

[21] Borelli, Giacomo, et al. “Mission analysis and guidance and control for the SpEye inspection CubeSat.” *Acta Astronautica 220* (2024): 75-87.

[22] Montenbruck, Oliver, et al. “E/I-vector separation for safe switching of the GRACE formation.” *Aerospace Science and Technology 10.7* (2006): 628-635.

[23] Gaias, Gabriella, and Jean-Sébastien Ardaens. “Flight demonstration of autonomous noncooperative rendezvous in low earth orbit.” *Journal of Guidance, Control, and Dynamics 41.6* (2018): 1337-1354.

[24] Borelli, Giacomo, Gabriella Gaias, and Camilla Colombo. “Rendezvous and proximity operations design of an active debris removal service to a large constellation fleet.” *Acta Astronautica 205* (2023): 33-46.

[25] Capuano, Vincenzo, et al. “VINAG: A highly integrated system for autonomous on-board absolute and relative spacecraft navigation.” *4S Symposium*. 2018.

[26] D’Amico, Simone, and Oliver Montenbruck. “Differential GPS: An enabling technology for formation flying satellites.” *Small Satellite Missions for Earth Observation: New Developments and Trends*. Springer Berlin Heidelberg, 2010.

[27] “Psiaki, Mark L., and Shan Mohiuddin. “Relative navigation of high-altitude spacecraft using dual-frequency civilian CDGPS.” *Proceedings of the 18th International Technical Meeting of the Satellite Division of The Institute of Navigation (ION GNSS 2005)*. 2005.

[28] Mohiuddin, Shan, and Mark L. Psiaki. “High-altitude satellite relative navigation using carrier-phase differential global positioning system techniques.” *Journal of Guidance, Control, and Dynamics 30.5* (2007): 1427-1436.

[29] Reichert, A., T. Meehan, and T. Munson. “Toward decimeter-level real-time orbit determination: a demonstration using the SAC-C and CHAMP spacecraft.” *Proceedings of the 15th International Technical Meeting of the Satellite Division of The Institute of Navigation (ION GPS 2002)*. 2002.

[30] Bonin, Grant, et al. “CanX–4 and CanX–5 precision formation flight: Mission accomplished!.” (2015).

[31] Flight results from the CanX-4 and CanX-5 formation flying mission

[32] Bertiger, W., et al. “GRACE: millimeters and microns in orbit.” *Proceedings of the 15th International Technical*

Meeting of the Satellite Division of The Institute of Navigation (ION GPS 2002). 2002.

[33] Kroes, Remco. "Precise relative positioning of formation flying spacecraft using GPS." (2006): 0768-0768.

[34] Capuano, Vincenzo, et al. "Feasibility study of GNSS as navigation system to reach the Moon." *Acta Astronautica 116* (2015): 186-201.

[35] Capuano, Vincenzo. "GNSS-based navigation for lunar missions". *No. 7130. EPFL*, 2016.

[36] Powe, M., et al. "Analysis of the international space station multipath and masking environment for automated transfer vehicle relative gps rendezvous manoeuvres." *2012 6th ESA Workshop on Satellite Navigation Technologies (Navitec 2012) & European Workshop on GNSS Signals and Signal Processing. IEEE*, 2012.

[37] Gaylor, David E., E. Glenn Lightsey, and Kevin W. Key. "Effects of multipath and signal blockage on GPS navigation in the vicinity of the International Space Station (ISS)." *Navigation 52.2* (2005): 61-70.

[38] Klein, Viliam, and Penina Axelrad. "Advanced multipath modeling and validation for GPS onboard the International Space Station." *Navigation 66.3* (2019): 559-575.

[39] Hwu, Shian U., and Y. C. Loh. "Space station GPS multipath analysis and validation." *1999 IEEE 49th Vehicular Technology Conference (Cat. No. 99CH36363)*. Vol. 1. IEEE, 1999.

[40] Teunissen, P. J. G. "Theory of carrier phase ambiguity resolution." *Wuhan University Journal of Natural Sciences 8* (2003): 471-484.

[41] De Jonge, Paul, and C. C. J. M. Tiberius. "The LAMBDA method for integer ambiguity estimation: implementation aspects." *Publications of the Delft Computing Centre, LGR-Series 12.12* (1996): 1-47.

[42] Nakka, Yashwanth Kumar, et al. "Information-based guidance and control architecture for multi-spacecraft on-orbit inspection." *Journal of Guidance, Control, and Dynamics 45.7* (2022): 1184-1201.

[43] Borelli, G., Gaias, G. V. M., & Colombo, C. "Safe guidance scheme for proximity operations forced motion". Accepted for publication in *Journal of Guidance, Control, and Dynamics. http://dx.doi.org/10.2514/1.G008179.* (2024)

[44] Borelli, Giacomo, G. V. M. Gaias, and Camilla Colombo. "Safety in forced motion guidance for proximity operations based on relative orbital elements." *33rd AAS/AIAA Space Flight Mechanics Meeting*. 2023.

[45] Ibarra-Castanedo, Clemente, et al. "Infrared image processing and data analysis." *Infrared physics & technology 46.1-2* (2004): 75-83.

[46] Hou, Fujin, et al. "Review on infrared imaging technology." *Sustainability 14.18* (2022): 11161.

[47] Downunder35m. "3D Scanning (Photogrammetry) With a Rotating Platform - Not a Rotating Camera!". *Instructables, 3D Printing* (2015)

[48] Datasets — COLMAP 3.8-dev documentation

[49] Piermattei, Livia. "The Use of Structure from Motion Technologies for High-Resolution Terrain Modelling on High Altitude CatchMents". (2016)

[50] Capuano, Vincenzo, et al. "Monocular-based pose determination of uncooperative space objects." *Acta Astronautica 166* (2020): 493-506.

[51] Capuano, V., Kim, K., Hu, J., Harvard, A., & Chung, S. J. (2018, October). Monocular-based pose determination of uncooperative known and unknown space objects. In *69th International Astronautical Congress (IAC)* (pp. 1-5). Paris, France: International Astronautical Federation (IAF).

[52] Karami, Ebrahim, Siva Prasad, and Mohamed Shehata. "Image matching using SIFT, SURF, BRIEF and ORB: performance comparison for distorted images." *arXiv preprint arXiv:1710.02726* (2017).

[53] Marelli, Davide, et al. "A Blender plug-in for comparing Structure from Motion pipelines." *2018 IEEE 8th International Conference on Consumer Electronics-Berlin (ICCE-Berlin)*. IEEE, 2018.

[54] Zhang, Haopeng, Quanmao Wei, and Zhiguo Jiang. "3D reconstruction of space objects from multi-views by a visible sensor." *Sensors 17.7* (2017): 1689.

[55] IEC TS 62446-3 "Photovoltaic modules and plants – Outdoor infrared thermography"

[56] Leccese, G., A. Fedele, and S. Natalucci. "Overview and roadmap of italian space agency activities in the micro- and nano-satellite domain." *73rd International Astronautical Congress (IAC)*. 2022.